Understanding the Reactivity, Selectivity and Deactivation of Frustrated Lewis Pairs for Semihydrogenation of Acetylene

Jingyun Ye[1,2,*], Megan McEwen[2]

[1]Department of Chemistry and Biochemistry, Duquesne University, Pittsburgh, Pennsylvania 15282, USA

[2]Department of Chemistry and Biomolecular Science, Clarkson University, Potsdam, New York 13699, USA

Corresponding author:

Jingyun Ye: yej1@duq.edu

Abstract: A good catalyst for semihydrogenation of alkynes must preclude both over-hydrogenation of alkene to alkane and isomerization to the other alkene isomer. In addition, it should balance the trade-off between selectivity and activity. In 2013, the Repo and Pápai groups reported a frustrated Lewis pair (FLP) (1-NMe_2-2-$B(C_6F_5)_2$-C_6H_4), **1**, which is a metal-free catalyst and for the first time shows excellent reactivity for the hydrogenation of internal alkynes. However, it is unreactive for terminal alkynes. In this work, we have designed thirteen FLPs, **a**−**m**, based on **1** by varying the Lewis base site with N and P, and the Lewis acid site with B, Al, Ga, and In, and replacing pentafluorophenyl with 1,3,5-trifluorophenyl, phenyl, or trifluoromethyl. We apply density functional theory to study the activity, selectivity, and deactivation of FLP **1**-**m** for acetylene semihydrogenation. The catalytic cycle consists of three steps: (1) alkyne insertion, (2) H_2 heterolysis, and (3) intramolecular protonation. We found the activity does not change much by the modification of bulky ligands, while it decreases with the direct replacement of LA and LB sites. The overall activity depends on steps 1 and 3, which are respectively positively and negatively linear correlated with the charge of Lewis acid site. Most of FLPs in this work show comparable or better selectivity for semihydrogenation of acetylene than of **1**. FLPs deactivation is due to the strong binding of acetylene and the elimination of electron-withdrawing bulky ligands at the pre-activated catalyst rather than at activated catalysts. Taking the selectivity and the stability of FLPs into account, we predict **d** and **k** are potentially active for terminal alkynes.

1. Introduction

Selective semihydrogenation of alkynes to alkenes is an important step in industrial polymerization processes from alkene monomers such as ethene, styrene, propylene, etc.[1–9] Ethene is a key building block in plastic, vital to the manufacturing industry.[10] Raw ethene is commercially produced from petroleum by catalytic cracking which generally contains trace amounts of acetylene that are poisonous to the Ziegler–Natta catalysts used for polymerization.[11–13] To avoid downstream catalyst poisoning, acetylene in the stream must be reduced to less than 5 ppm prior to polymerization.[8,14,15] One strategy to achieve this requirement is to use supported Pd catalysts for acetylene semihydrogenation such as Lindlar's catalyst. This commercial catalyst, developed in 1952, still is widely used for industrial semihydrogenation of alkynes to *Z*-alkenes.[16] However, its disadvantages—the high cost of Pd, the low selectivity to alkene, and potential harm to the environment and human health if lead is introduced into the waste stream, motivate research efforts to replace Lindlar's catalyst. Research efforts have sought to control the shape of Pd nanoparticle,[17] prepare isolated single-atom catalysts,[18–22] modify the supports,[23–33] alloy Pd with a second metal,[34–38] use organic modifiers[39,40], or use bimetallic dual site catalysts[41,42]. Although significant progress has been achieved, new catalysts predominantly use expensive noble-metals (e.g., Pd[18-40], Pt[43], Ru[44], Rh[42], Au[38], Ag[35]) and their related alloys with gaseous hydrogen (H_2) or expensive and/or toxic organic hydrogen sources. Thus, these alternatives raise new concerns pertaining to cost, safety, and sustainability. Therefore, developing low-cost (metal-free), environmentally friendly, highly active and highly selective catalysts for selective semihydrogenation of alkyne to alkene is of great importance.

Frustrated Lewis pairs (FLPs) are simply the combination of a bulky Lewis acid (LA) and a bulky Lewis base (LB) sterically precluded from forming classical Lewis acid-base adducts. In this fashion, the unquenched LA and LB sites are available to accept and donate electrons, respectively, providing a unique route to activate small molecules for applications in catalysis.[45–48] In 2013, the Repo and Pápai groups reported a FLP based on ambiphilic aminoborane, 1-NMe_2-2-$B(C_6F_5)_2$-C_6H_4, **1** (**Figure 1**), which is metal-free catalyst and shows excellent reactivity for the hydrogenation of internal alkynes (up to 100% conversion).[49] However, it is unreactive for terminal alkynes or alkynes comprising a terminal double bond, which was attributed to C-H bond cleavage of terminal alkynes or strong binding of alkynes with terminal double bonds results the catalyst degradation.[49] Selective semihydrogenation of terminal alkyne is of great interest but it is

still a significant challenge because many reactions compete with the production of the targeted product, alkene. Therefore, the discovery of FLPs with high activity and selectivity for semihydrogenation of the terminal alkynes or alkynes with terminal double bonds without the catalyst degradation would be great improvement to polymer industry.

A good catalyst for semihydrogenation of alkynes must preclude both over-hydrogenation of the alkene to alkane and isomerization to the other alkene isomer, in addition, balance the trade-off between selectivity and activity. In this work, we have designed thirteen FLPs (**a**−**m** as shown in **Figure 1**) based on **1** by varying the LB site with N and P, and the LA site with B, Al, Ga and In, and replacing the bulky ligands (LG) pentafluorophenyl (−C_6F_5) with 1,3,5-trifluorophenyl (−$C_6F_3H_2$), phenyl (−C_6H_5), trifluoromethyl (−CF_3). We sought to understand the activity, selectivity and the deactivation of FLPs **1**−**m** for semihydrogenation of acetylene**,** with the goal of identify the FLP candidates with good selectivity and activity for the semihydrogenation of acetylene without suffering the FLP degradation. The quantitative characterization of structure-reactivity relations had been analyzed to gain deeper insight into the reactivity-determining factors for the prediction and design of FLPs with ideal catalytic performance for terminal alkyne semihydrogenation. More importantly, the reaction mechanism for the deactivation of FLPs by acetylene has been investigated in detail, which allows us to predict the FLP candidates with good stability when exposed to terminal alkynes and develop efficient strategies to improve the stability of FLPs for terminal alkynes semihydrogenation.

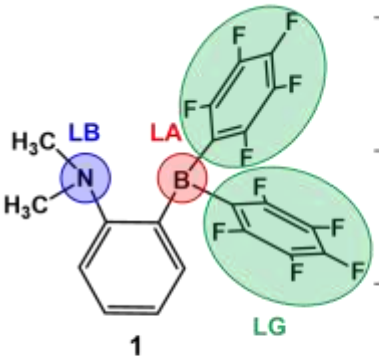

FLP	LB	LA	LG
1	N	B	C_6F_5
a	N	Al	C_6F_5
b	N	Ga	C_6F_5
c	N	In	C_6F_5
d	P	B	C_6F_5
e	P	Al	C_6F_5
f	P	Ga	C_6F_5
g	P	In	C_6F_5
h	N	B	$C_6F_3H_2$
i	N	B	C_6H_5
j	N	B	CF_3
k	P	B	$C_6F_3H_2$
l	P	B	C_6H_5
m	P	B	CF_3

Figure 1. Structure of the 2-[bis(pentafluorophenyl)boryl]-*N*,*N*-dialkylanilines, **1** and a family of FLPs (**a**-**m**) designed by modify the Lewis acid site (in red circle), Lewis base site (in blue circle), and the bulky ligands (in green circles) of **1**.

2. Computational Method

Gaussian 16[50] calculations were performed with the hybrid meta exchange-correlation functional M06-2X[51] using a def2-TZVP basis set for atoms.[52,53] The structures of all species were optimized in the gas phase. Harmonic vibrational frequencies were computed to confirm the nature of all intermediates (no imaginary frequencies) and transition state structures (one imaginary frequency). The gas-phase Gibbs free energies, *G*, were calculated at T = 298.15 K and 1 atm pressure by using the harmonic approximation for the optimized structures. The solvation effect of benzene, the solvent used in the experiment[49], was included by performing single-point energy calculations at the gas-phase geometries using the SMD solvation model.[54] The relative solution-phase Gibbs free energies were calculated by adding solvation energies to the gas-phase relative Gibbs free energies. The Cartesian coordinates of all the structures and their associated electronic energies, enthalpies, and Gibbs free energies in both the gas phase and in solution are given in the Supporting Information. The energy values reported in the main text are Gibbs free energies (298.15 K, standard state of 1 atm for gases and 1 M for solutes) including the solvent effect of benzene. Partial atomic charges were calculated for the gas phase molecules using CM5 charge model developed by Truhlar and coworkers.[55] We tested M06-L[56] since it is also recommended for main-group and transition element, but which is found to underestimate the barrier heights (**Table S1-S2**). We calculated the free energies by scaling the harmonic frequency.[57] We found the absolute value of free energies do change when scale factor was considered, however, it does not change the trend (**Table S3**).

The bonding and electron density deformation were analyzed by using natural orbitals for chemical valence (NOCV)[58–60] combined with the energy decomposition analysis (EDA)[61,62,63] implemented in the Amsterdam density functional (*ADF*) program.[64–66] The M06-2X[51] functional and TZP[67] all-electron basis set were used for ETS-NOCV calculations with the optimized geometries described above carried out with *Gaussian 16*. The introduction of EDA−NOCV method is available in our previous publication[68].

3. Results and Discussion

3.1 Reaction Mechanism

The classical mechanism of FLP-catalyzed the hydrogenation of C-C multiple bonds involves the heterolytic cleavage of H_2 and then transfer the hydride and the proton to C–C multiple

bonds in sequence or in a concerted fashion. However, this classical mechanism is restricted to alkene hydrogenation under ambient condition. Therefore, a new reaction mechanism was proposed by Repo and Pápai et al,[49] which is demonstrated in **Figure 2**, where we show the semihydrogenation of acetylene, the targeted reaction in this work, as an example. Compound **1** is a pre-catalyst, which needs to be activated by H_2 before the hydrogenation of alkynes or alkenes. The pre-activation involves **1** to undergo a FLP mechanism that the heterolytic cleavage of H_2 to produce **2** with the hydride bound to LA site (B) and the proton bound to LB site (N), and then followed by the intramolecular protonative cleavage of B–C_6F_5 to eliminate 1,2,3,4,5-pentafluorobenzene (C_6F_5H) and produce **3** which is the catalyst that is responsible for hydrogenation of alkynes and akenes. Subsequently, the introduction of alkynes leads to two possible reaction pathways: path A, alkyne hydrogenation to alkene and path B, alkene hydrogenation to alkane. Each pathway comprises three steps: (1) ***alkyne/alkene insertion***, insertion of the C≡C (or C=C) functionality into the B−H bond to form a vinyl, **4** (or alkyl, **6**); (2) ***H_2 heterolysis***, the heterolytic cleavage of H_2 to produce **5** (or **7**) by FLP mechanism; (3) ***intramolecular protonation***, a proton transfer from LB site to vinyl (or alkyl) species and release alkene (or alkane), liberating the catalyst **3**, and the full catalytic cycle is completed.

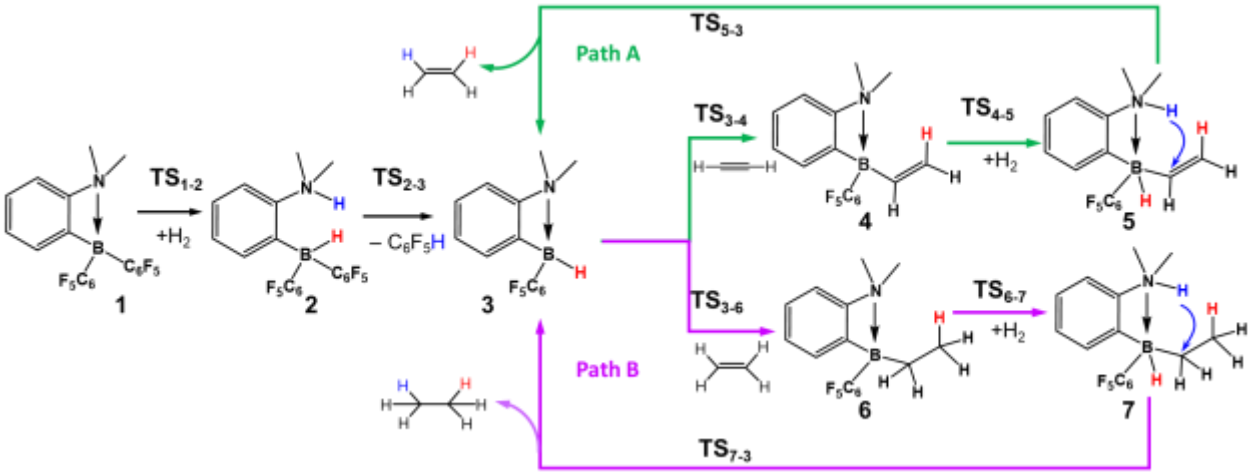

Figure 2. Mechanism of semihydrogenation of acetylene catalyzed by **1**: pre-catalyst activation by H_2 (in black), hydrogenation of acetylene into ethene (path A in green) and hydrogenation of ethene to ethane (path B in purple).

3.2 Activity and Selectivity

Compound **1** is capable of hydrogenation of a variety of alkynes to alkenes except terminal alkynes or alkynes comprising a terminal double bond.[49] In this work, we focus on the exploration the potential FLPs that able to selectively hydrogenate terminal alkynes, acetylene in particular. Density Functional Theory (DFT) calculations were carried out to locate the intermediates and transition states along the reaction pathway and the energetic span model developed by Kozuch and Shaik[69,70] was used to predict the overall activation free energies and turnover frequency to determine their activity and selectivity for the semihydrogenation of acetylene to ethene catalyzed by FLPs **1**-**m**. The details about energetic span model and TOF data (**Table S4**) are provided in SI. It is well known that it is challenging for quantum chemistry to predict absolute rate constants. A 2 kcal/mol error in a free energy of activation changes will result in the calculated rate constant by a factor of 30 and a 5.5 kcal/mol error changes it by a factor of 10^4. In addition, the reaction conditions such as pressure, concentration of the catalysts, solubility of reactant will affect the overall reaction rate. Another reason is that the calculated TOFs correspond to ideal conditions without side reactions or catalyst poisoning. In addition, we should keep in mind that the TOFs are calculated here from standard-state free energies, which differ from the free energy changes under experimental conditions. Therefore, our focus is the apparent activation energies and the relative TOFs.

Figure 3a shows the Gibbs free energy profile of catalytic cycle for the hydrogenation of acetylene to ethene and ethene to ethane catalyzed by **d3**, which is activated from pre-catalyst **d**. Starting from **d3**, the first step involves acetylene insert to B hydride to form B-vinyl intermediate, **d4**, which is a highly exergonic step (−31.7 kcal/mol) with a relative small Gibbs free energy of activation (18.9 kcal/mol) via the transition state $\mathbf{TS_{d3\text{-}4}}$. Subsequently, H_2 is heterolytically split to a hydride bound to B and a proton bound to P. The H_2 heterolysis step is endergonic by 12.3 kcal/mol via the transition state $\mathbf{TS_{d4\text{-}5}}$ and the Gibbs free energy of activation is 27.1 kcal/mol respect to **d4**. The next intramolecular protonation step proceeds as the proton bound to P directly migrates to the vinyl substituent of **d5** via the transition state $\mathbf{TS_{d5\text{-}3}}$, leading to the elimination of ethene and regeneration of **d3**. The Gibbs free energy of activation of the intramolecular protonation step (22.2 kcal/mol relative to **d5**) is slightly higher than the acetylene insertion step (18.9 kcal/mol) and is exergonic by −15.8 kcal/mol (relative to **d5)**. According to the energetic span model, we identify the turnover frequency determining intermediate (TDI) and turnover frequency determining transition state (TDTS) are **d4** and $\mathbf{TS_{d5\text{-}3}}$, respectively. The apparent activation energy for acetylene hydrogenation to ethene ($\Delta G^{\ddagger}_{C\equiv C}$) is calculated to be 34.5 kcal/mol.

The potential energy profile for the hydrogenation of ethene to ethane lies above that of acetylene to ethene. The ethene insertion at **d3** has a slightly larger free energy barrier (20.5 kcal/mol) than that of acetylene insertion (18.9 kcal/mol). While the formation energy of alkyl substituent (-17.2 kcal/mol) of **d6** is greatly reduced comparing that of vinyl substituent (-31.7 kcal/mol) of **d4**. The H_2 heterolysis at **d6** ($\Delta G^{\ddagger}$ =27.2 kcal/mol, ΔG =13.0 kcal/mol) has a similar Gibbs free energy of activation and reaction with that at **d4**. For the last step, the intramolecular protonation transfer to alkyl substituent of **d7** ($\Delta G^{\ddagger}$ =28.1 kcal/mol) has larger free energy barrier than that to vinyl substituent of **d5** (22.2 kcal/mol) and the elimination of ethane (ΔG =−22.0 kcal/mol) is more thermodynamic favorable than that of ethene (−15.8 kcal/mol). The TDI and TDTS are **d6** and $\mathbf{TS_{d7\text{-}3}}$, respectively, and the apparent activation energy for ethene hydrogenation to ethane ($\Delta G^{\ddagger}_{C=C}$) is calculated to be 41.1 kcal/mol. The apparent activation energy for the hydrogenation of acetylene to ethene ($\Delta G^{\ddagger}_{C\equiv C}$ = 34.5 kcal/mol) is 6.6 kcal/mol lower than that for the hydrogenation of ethene to ethane ($\Delta G^{\ddagger}_{C=C}$ = 41.1 kcal/mol), corresponding to a turnover frequency (TOF) for the hydrogenation of acetylene to ethene ($TOF_{C\equiv C}$) is 5 orders magnitude larger than that for ethene to ethane ($TOF_{C=C}$), which suggests **d3** shows good selectivity for semihydrogenation of acetylene to ethene rather than to ethane.

A FLP catalyst that is selective for the hydrogenation of acetylene to ethene over ethane should have $\Delta G^{\ddagger}_{C\equiv C}$ smaller than $\Delta G^{\ddagger}_{C=C}$ (or $TOF_{C\equiv C} > TOF_{C=C}$). Therefore, $\Delta G^{\ddagger}_{C\equiv C}$ and $\Delta G^{\ddagger}_{C=C}$ for **3-m3** are plotted in **Figure 3b** for comparison and the Gibbs free energy profiles for each catalyst is provided in **Figures S1-S13**. We found that all the FLPs designed in this work show comparable or better selectivity for semihydrogenation of acetylene comparing to **3**, except **b3** and **c3**, for which the energy difference between $\Delta G^{\ddagger}_{C\equiv C}$ and $\Delta G^{\ddagger}_{C=C}$ is too small (≤ 1 kcal/mol) and the corresponding $TOF_{C\equiv C}$ and $TOF_{C=C}$ are in the same order of magnitude ($TOF_{C\equiv C}/TOF_{C=C}$ = 6 for b3 and 1 for c3 as shown in Table S4) indicating the low selectivity.

For the activity of FLPs toward acetylene and ethene hydrogenation, we found that the direct replacement of LA and LB sites has a greater impact on the activity than modifying the LG. As shown in **Figure 3b**, when the LA site, B of **3** and **d3** is replaced with Al, Ga and In, $\Delta G^{\ddagger}_{C\equiv C}$ changes -1.8 to 5.6 kcal/mol and $\Delta G^{\ddagger}_{C=C}$ changes -5.6 to 3.4 kcal/mol. When the LB site, N of FLPs (**3-c3**, **h3-j3**) is replaced with P (**d3-g3** and **k3-m3**), $\Delta G^{\ddagger}_{C\equiv C}$ increases 2.1 to 8.1 kcal/mol and $\Delta G^{\ddagger}_{C=C}$ increases 1.1 to 10.1 kcal/mol, indicating FLPs with N as LB site (LA-N FLPs) have higher activity than FLPs with P as LB site (LA-P FLPs) for the hydrogenation of acetylene and

ethene. For N-B FLP family (**3**, **h3-j3**), $\Delta G^{\ddagger}_{C\equiv C}$ and $\Delta G^{\ddagger}_{C=C}$ increase 0.1~0.5 kcal/mol when $-C_6F_5$ of **3** is replaced with $-C_6F_3H_2$ or $-C_6H_5$, while $\Delta G^{\ddagger}_{C\equiv C}$ and $\Delta G^{\ddagger}_{C=C}$ decrease 2.2 kcal/mol and 3.0 kcal/mol, respectively when $-C_6F_5$ is replaced with $-CF_3$. The similar trend is identified for P-B FLP family. $\Delta G^{\ddagger}_{C\equiv C}$ and $\Delta G^{\ddagger}_{C=C}$ for P-B FLP family (**d3**, **k3-m3**) changed −0.1~0.3 kcal/mol when the bulky ligand $-C_6F_5$ of **d3** is replaced with $-C_6F_3H_2$ or $-C_6H_5$, however, which decreased 1.3 kcal/mol and 1.4 kcal/mol, respectively when $-C_6F_5$ is replaced with $-CF_3$.

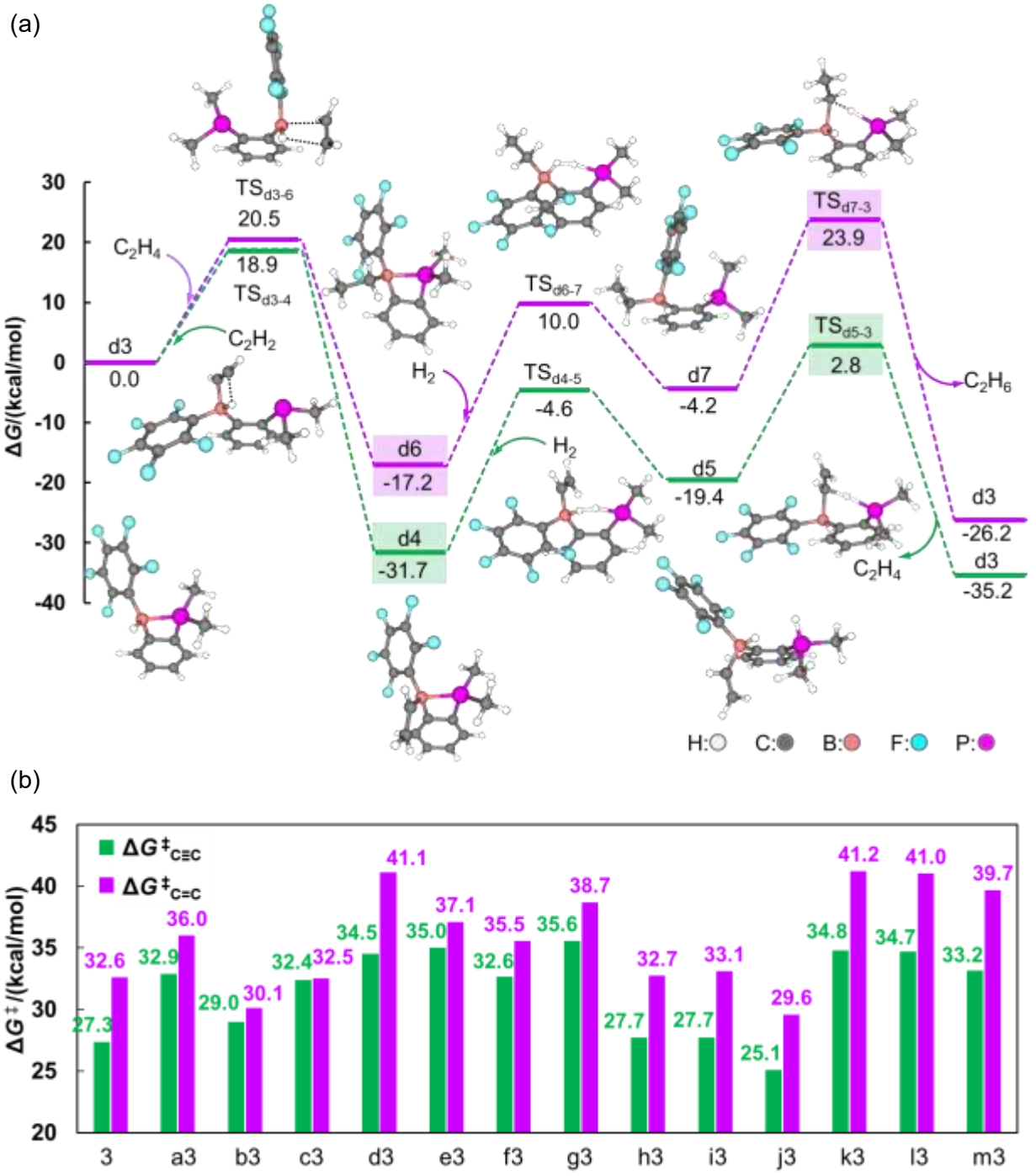

Figure 3. (a) the Gibbs free energy profiles for the hydrogenation of acetylene to ethene (green line) and ethene to ethane (purple line) catalyzed by **d3**, with TDI and TDTS highlighted in the green or purple boxes and the structures represented in ball and stick format. (b) the apparent activation free energies for acetylene hydrogenation to ethene ($\Delta G^{\ddagger}_{C\equiv C}$) and ethene hydrogenation to ethane ($\Delta G^{\ddagger}_{C=C}$) catalyzed by **3**-**m3**.

To understand the factors that govern the reactivity of FLPs toward acetylene/ethene hydrogenation, partial atomic charges, HOMO, LUMO, HOMO-LUMO gap, fluoride ion affinity (FIA), hydride affinity (HIA) and the bond length of LA-LB sites of **3**-**m3** have been analyzed and the data is summarized in **Table S5**. **Figure 4a** and **4b** show the charges of LA site and LB site of **3**-**m3**. We found the charge of LA site increases dramatically when replacing B with Al, Ga and In for LA(C_6F_5)-N FLPs (red solid line) and LA(C_6F_5)-P FLPs (red dash line). However, the modification of the ligand $-C_6F_5$ with $-C_6F_3H_2$, $-C_6H_5$ or $-CF_3$ has little effect on the charges of LA site for B(LG)-N FLPs (black solid line) and B(LG)-P FLPs (black dash line). In addition, we found replacing of LB site of N with P reduces CM5 charge of LA site, as shown in **Figure 4a** that dash lines shift downwards slightly compared to the solid lines. The modification of LA site and ligands has minor effect on the charges of LB site as shown in **Figure 4b**.

The charge analysis suggests the charge of LA site is greatly affected by replacing B with Al, Ga and In, is weakly affected by replacing the LB site of N with P, is barely affected by the ligand modification. The impact of the modification of LA/LB site and LG on the charge of LA is consistent with that on the apparent activation energies. Therefore, we explored the relations between the reactivity and the charge of LA site of FLPs (**3**-**m3**). We have tried to correlate the apparent activation energies ($\Delta G^{\ddagger}_{C\equiv C}$ and $\Delta G^{\ddagger}_{C=C}$) with CM5 charges of LA site and all the other descriptors, but failed to identify good linear relationships (**Figure S14**). The bad correlation is because TDI and TDTS are not consistent for all FLPs (**Figures S1-S13**). For **3**, **a3** and **e3**-**m3**, $\Delta G^{\ddagger}_{C\equiv C} = G_{TS5\text{-}3} - G_4$ because TDI and TDTS are **4** and $TS_{5\text{-}3}$ for acetylene hydrogenation, and $\Delta G^{\ddagger}_{C=C} = G_{TS7\text{-}3} - G_6$ because TDI and TDTS are **6** and $TS_{7\text{-}3}$ for ethene hydrogenation. For **b3** and **c3,** $\Delta G^{\ddagger}_{C\equiv C} = \Delta G^{\ddagger}_{3\text{-}4}$ because TDI and TDTS are 3 and $TS_{3\text{-}4}$ for the acetylene hydrogenation. We found that **4** (or **6**) and $TS_{4\text{-}5}$ (or $TS_{6\text{-}7}$) are the intermediate and transition state have lowest free energy along the reaction path for each FLP (see **Tables S6**-**S7**, **Figures S15**-**S16**). Therefore, the apparent activation energies do not depend on step 2, ***H_2 heterolysis***, but depend on step 1, ***alkyne insertion***, **3** → **4** (or **3** → **6**) and step 3, ***intramolecular protonation***, **5** → **3** (or **7** → **3**). For acetylene hydrogenation, we plotted the free energy barriers of step 1 ($\Delta G^{\ddagger}_{x3\text{-}4}$) and step 3 ($\Delta G^{\ddagger}_{x5\text{-}3}$) as a function of the CM5 charge of LA site of **3**-**g3** (**h3**-**m3** was not included because the effect of ligand modification is neglectable, the free energies for each elementary step are listed in **Tables S8**-**S9**), which gives two linear relationships with a coefficient of determination of $R^2 = 0.86$ and $R^2 = 0.75$, respectively, (**Figure 4c**). Linear relationships between $\Delta G^{\ddagger}_{x3\text{-}6}$ (or $\Delta G^{\ddagger}_{x7\text{-}3}$) and the CM5

charge of LA site have also identified for ethene hydrogenation as well, which gives a coefficient of determination of $R^2 = 0.83$ and $R^2 = 0.87$, respectively.

For the alkyne insertion step, the free energy barriers ($\Delta G^{\ddagger}_{x3\text{-}4}$ or ($\Delta G^{\ddagger}_{x3\text{-}6}$) increase when the charge of LA site becomes more positively charged. To understand the correlation between $\Delta G^{\ddagger}_{x3\text{-}4}$ of step 1 and charge of LA site, the electronic character of the bonding between C_2H_2 and **3** of $TS_{3\text{-}4}$ were analyzed using the EDA-NOCV scheme. **Figure 4e** and **4f** present the two leading NOCV deformation densities ($\Delta\rho_1$ and $\Delta\rho_2$) contribute to the total interaction orbital energies (ΔE_{orb}). As we can see, the contribution from the first NOCV deformation densities, $\Delta\rho_1$, presented in **Figure 4e**, clearly demonstrates the electron transfer from the π bonding orbital of C≡C to the empty δ orbital of B-C (π donation: $\pi_{C\equiv C} \rightarrow \delta_{B\text{-}C}$), and the total charge transfer corresponding to $\Delta\rho_1$ is 0.82. The second NOCV deformation density contribution, $\Delta\rho_2$ (**Figure 4f)** shows the electron density donation from the δ bonding orbital of B-H bond to the π anti-bonding orbital of C≡C (δ back-donation: $\delta_{B\text{-}H} \rightarrow \pi^*_{C\equiv C}$), and the total charge transfer corresponding to $\Delta\rho_2$ is 0.41. In addition, we found that electron out flows from $\delta_{B\text{-}H}$ bonding orbital for both $\Delta\rho_1$ and $\Delta\rho_2$, indicating the weakening of B-H bond and the potential of H migration to C_2H_2. The stabilizing orbital interaction energy from the first and second pair of NOCV are 88.6 kcal/mol and 23.5 kcal/mol, which contribute to 69.9% and 18.5 % of the total orbital interaction energy, respectively. The orbital interaction energy analysis suggests the dominant contribution to the orbital interaction energy of $TS_{3\text{-}4}$ comes from the π donation charge transfer ($\pi_{C\equiv C} \rightarrow \delta_{B\text{-}C}$). More positively charged of LA site means stronger ability to accept electrons. Therefore, a FLP with a more positively charged LA site has a stronger π donation from C≡C of C_2H_2 to FLP and weaker δ back-donation from FLP to $\pi^*_{C\equiv C}$ of C_2H_2, resulting in stronger binding of C_2H_2 at B, but less activated C≡C for hydrogenation, in another word, higher activation barrier.

Intramolecular protonation is an electrophilic attacking reaction, which involves the intramolecular protonation migrate to carbon (bound to LA) of vinyl intermediate, and the free energy barrier ($\Delta G^{\ddagger}_{x5\text{-}3}$) is expected to depend on the charge of proton and carbon atom of vinyl intermediate of **5**, which are ultimately affected by the charge of LA and LB sites of **5**. From the charge analysis (**Table S10**), the charge of proton (+0.28 ~ +0.32 e) does not change much when LA is varied from B to Al, Ga and In for **5-c5,** which is because of the almost the same charge of LB site (-0.35 e) for **5-c5**. Therefore, the charge of proton or LB site is excluded as a descriptor to correlate with $\Delta G^{\ddagger}_{x5\text{-}3}$. On the other hand, we found that the charge of carbon of vinyl decrease

with the increase of the charge of LA site. To understand the charge transfer between vinyl species and B of **5**, the EDA-NOCV scheme were analyzed for **5**. As shown in **Figure 4g**, the dominant NOCV deformation densities ($\Delta\rho_1$) demonstrate the electron transfer from the π bonding orbital of C=C of vinyl to the δ orbital of B-C (π donation: $\pi_{C=C} \rightarrow \delta_{B\text{-}C}$), and the total charge transfer corresponding to $\Delta\rho_1$ is 0.86. The dominant NOCV deformation densities ($\Delta\rho_1$) contribute to 77.9% of $\Delta E_{\mathrm{orb}}$of **5**, and the second dominant NOCV deformation densities ($\Delta\rho_2$) is not included in the discussion because its contribution to B-vinyl bond is small, only counts for 6% of ΔE_{orb}. A stronger electron donation from vinyl species to LA site, suggests a stronger B-C bond, which will require to overcome a higher free energy barrier to be protonated. This explains the correlation between $\Delta G^{\ddagger}_{x5\text{-}3}$ and the charge of LA with negative slop in **Figure 4c**: a more positively charged LA site indicate weaker electron donation from vinyl species to LA site, resulting in a weaker LA-C bond, then a smaller free energy barrier for proton transfer to vinyl species to form ethene.

The a similar relationships observed for $\Delta G^{\ddagger}_{x3\text{-}6}$ and $\Delta G^{\ddagger}_{x7\text{-}3}$ as a function of the charge of LA (**Figure 4d**) is because the interaction and charge transfer between alkyne/alkene and LA, vinyl/alkyl and LA are similar.

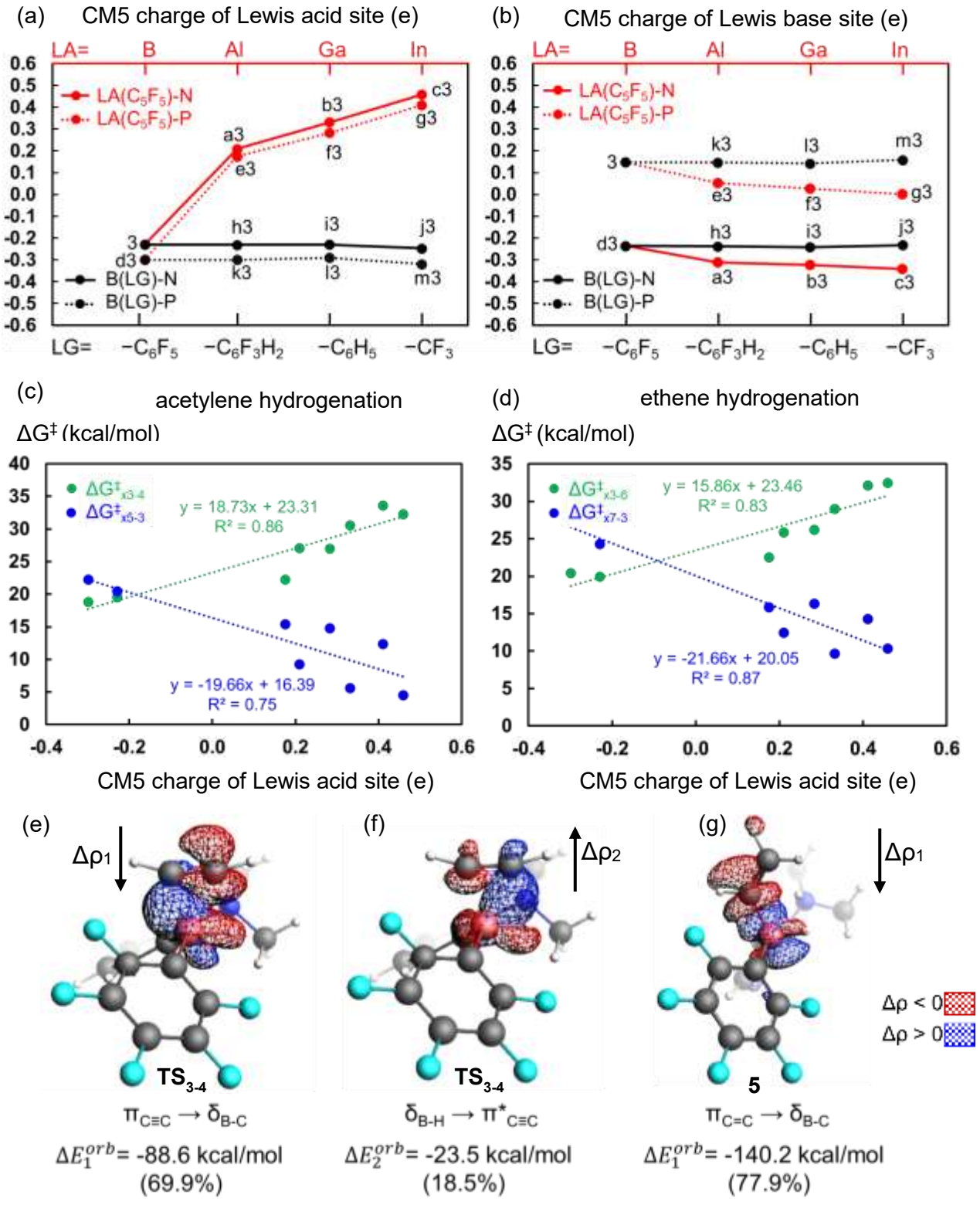

Figure 4. CM5 charge of FLP catalyst **3-m3**: (a) Lewis acid site and (b) Lewis base site. Red solid and dash lines represent LA(C_6F_5)-N FLP family (**3**, **a3**, **b3** and **c3**, where the LA are B, Al, Ga

and In, respectively and the LB is N) and LA(C_6F_5)-P FLP family (**d3**, **e3**, **f3** and **g3**, where the LA are B, Al, Ga and In, respectively and the LB is P). Black solid and dash lines represent B(LG)-N FLP family (**3**, **h3**, **i3** and **j3**, where the LA and LB are B and N, respectively) and B(LG)-P FLP family (**d3**, **k3**, **l3** and **m3**, where the LA and LB are B and P, respectively) and their bulky ligands are varied from $-C_6F_5$ to $-C_6F_3H_2$, $-C_6H_5$ or $-CF_3$. (c) and (d) calculated free energy barriers for step 1 and step 3 as a function of CM5 charge of LA site of **3**-**g3** for the hydrogenation of acetylene and ethene, respectively. (e) and (f) two leading deformation densities contribute to the interaction energies between acetylene and **3** of **TS**$_{3\text{-}4}$, and (g) the dominant deformation densities contribute to the interaction energies between vinyl species and B of **5** (red color shows charge outflow, $\Delta\rho < 0$, whereas the blue color shows charge accumulation, $\Delta\rho > 0$).

3.3 Catalyst Deactivation

The lack of reactivity of **1** to hydrogenate terminal alkynes was attributed to the strong binding of terminal alkynes with the boron of **1** causing the degradation of the catalyst via a deprotonative borylation pathway.[49,71–76] To improve the activity of FLP catalysts toward terminal alkynes requires more detailed reaction mechanism studies for the catalyst degradation, which can occur prior to or after the activation of the pre-catalysts by H_2, as shown in **Figure 5** and **Figure 6**, respectively.

Starting with pre-catalyst **1**, there are two competitive reaction pathways in the presence of H_2 and acetylene: pre-catalyst activation and deactivation, as shown in **Figure 5a**. Pre-catalyst activation consists of two elementary steps: (i) H_2 heterolysis and (ii) perfluorophenyl elimination. H_2 heterolysis results the heterolytically splitting of H_2 and the formation of a hydride and a proton attached to LA and LB site respectively, **2**, via the transition state $TS_{1\text{-}2}$. The perfluorophenyl elimination step involve the transition state $TS_{2\text{-}3}$. Pre-catalyst deactivation also consists of two elementary steps: (iii) acetylene addition and (iv) perfluorophenyl elimination. Acetylene addition involves the cleavage of C-H bond of acetylene, resulting in the formation of **8** with an ethynide binding at LA (B) site and a proton binding at LB (N) site via the transition state $TS_{1\text{-}8}$, which is responsible for pre-catalyst deactivation, because the stronger binding of alkyne blocks the H_2 splitting. The intramolecular protonative cleavage of B–C_6F_5 could occur for **8** via the transition state of $TS_{8\text{-}9}$ to eliminate C_6F_5H and produce **9**, which is responsible for catalyst degradation because the active borohydride species no longer exists for propagate the alkyne hydrogenation.

Further H_2 splitting at **9** will result in the complete degradation of catalyst due to the second C_6F_5 group elimination. The Gibbs free energies of reaction and activation for the elementary steps (i-iv) involving in the pre-catalyst activation, deactivation and degradation for FLP **1**-**m** are plotted in **Figure 5b** and **5c** and the data are summarized in **Table S11**.

We found the activation and reaction free energies for the perfluorophenyl elimination step for pre-catalyst activation (ii) and degradation (iv) are close (**Figure 5c**), therefore, we focus on the Gibb's free energies of reaction and activation of the first step (i and iii) for pre-catalyst activation and deactivation. The Gibb's free energies of acetylene addition ($\Delta G_{x1\text{-}8}$) are much larger than that of H_2 heterolysis ($\Delta G_{x1\text{-}2}$), except for **d** and **k**, suggesting acetylene addition is thermodynamically much favorable than H_2 splitting due to the stronger binding of acetylene. While to determine if a FLP pre-catalyst is activated or deactivated, the free energy barriers which govern the kinetics of the reaction are considered as well. We identify that **a**-**c**, **e**-**g** and **j** would not be good catalysts, because both the Gibb's free energies of reaction ($\Delta G_{x1\text{-}8}$) and activation ($\Delta G^{\ddagger}_{x1\text{-}8}$) for acetylene addition are smaller than that of H_2 heterolysis ($\Delta G_{x1\text{-}2}$ and $\Delta G^{\ddagger}_{x1\text{-}2}$), suggesting the acetylene addition is thermodynamically and kinetically more favorable than H_2 heterolysis. For **1**, **d**, **h**, **i**, and **k**-**m**, the pre-catalyst activation and deactivation are competitive, because acetylene addition is thermodynamically favorable ($\Delta G_{x1\text{-}8} < \Delta G_{x1\text{-}2}$), while kinetically is less favorable ($\Delta G^{\ddagger}_{x1\text{-}8} > \Delta G^{\ddagger}_{x1\text{-}2}$). Previous experimental results show that the addition of the terminal alkyne results in the formation of alkyne adduct with **1**, which will follow by a full cleavage of C_6F_5 group upon heating with excess terminal alkyne under H_2 pressure, and resulting the pre-catalyst degradation.[49] Comparing to **1**, **h**, **i**, **l** and **m** will probably undergo the degradation like **1** because acetylene addition is exergonic or slightly endergonic while H_2 heterolysis is endergonic, and the acetylene binding is 3.9~9.2 kcal/mol lower than H_2 heterolysis. For **d** and **k**, the binding free energies of alkyne and H_2 are close and both endergonic, while the free energies barrier for acetylene addition is much higher (8.3~8.7 kcal/mol) than that of H_2 heterolysis. **d** and **k** could be potential pre-catalyst to reduce the FLP degradation because the kinetics will be the dominant factor rather than thermodynamics. To drive the reaction toward H_2 splitting, we can increase the temperature and pressure which will increase the reaction rate and result in the H_2 splitting is kinetically more favorable, or change solvent (e.g., The binding free energy decreases from -0.1 kcal/mol to -3.0 kcal/mol and the activation free energy increase from 20.5 kcal/mol to 21.0 kcal/mol for H_2 splitting at compound 1 when the solvent is changed from toluene to tetrahydrofuran). As supported

by the experimental results, the conversion of H_2 heterolysis catalyzed by compound **1** is found to be increased to 90% at 80ºC after 6h in the solvent C_6D_5Br and to 80% at 80ºC after 7h in the solvent toluene, and the reaction rate is increased 10 times when the H_2 pressure increased from 2 bar to 30 bar, while H_2 heterolysis is reversible at room temperature and 2 bar in the solvent C_6D_6.[49] We would like to emphasize that the activation and binding free energies in this work are calculated at 298.15 K and 1 atm which is lower than the experimental reaction condition 80 ºC and 2 bar [49]. In addition, the elimination of C_6F_5H is a great exergonic reaction for all the FLPs (Table S11) which could be another potential driving force to shift the reaction towards the H_2 splitting rather than releasing.

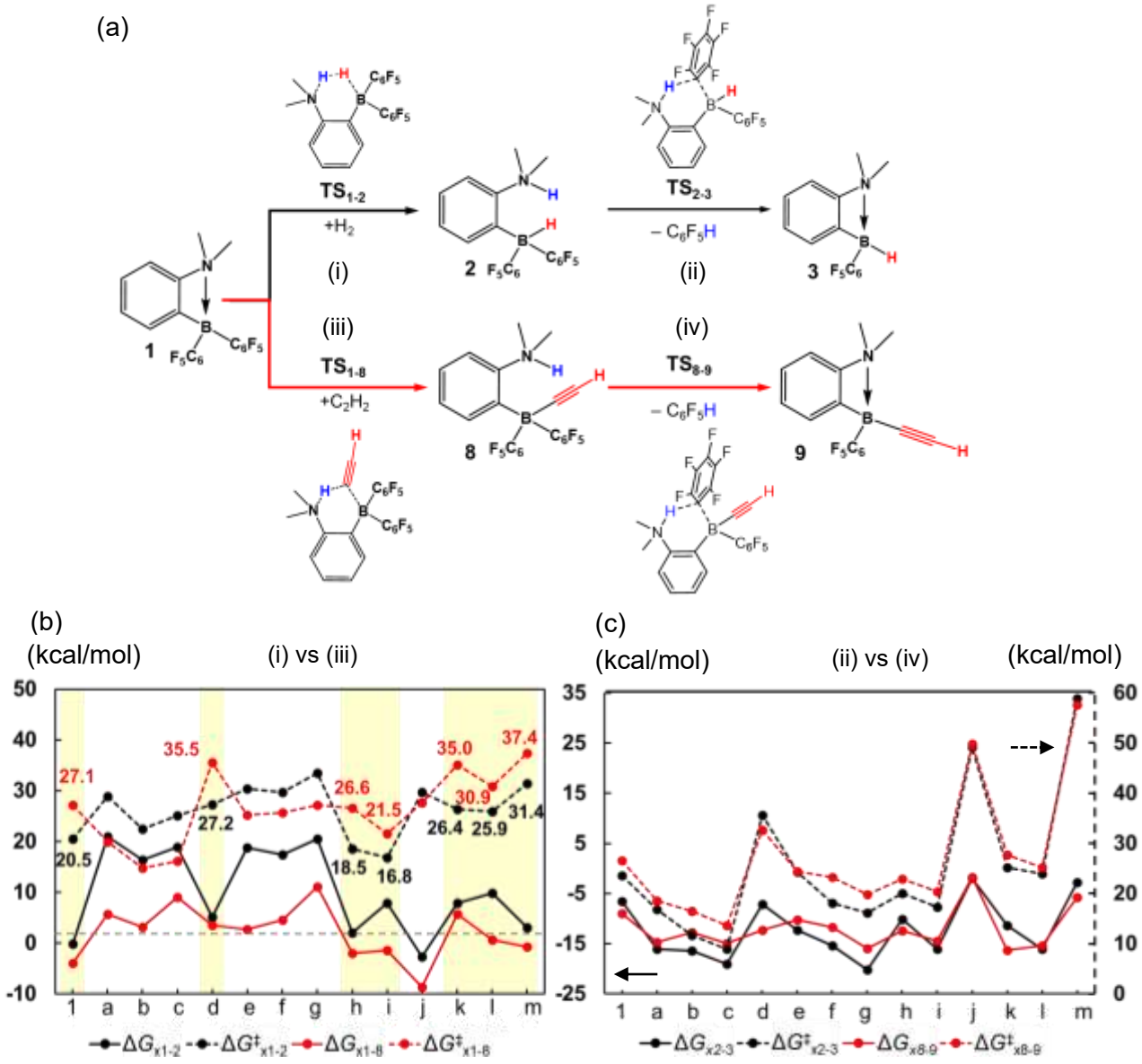

Figure 5. (a) The reaction mechanism for the activation and deactivation of pre-catalyst **1** by H_2 and acetylene, respectively, (b) and (c) are the Gibbs free energies of reaction and activation for each elementary steps involving in the pre-catalyst activation and deactivation for FLP **1**-**m**. x is none for **1**, and x = a-m for FLP **a**-**m**.

We have also explored the catalyst deactivation starting from the activated catalyst **3**−**m3** and the Gibbs free energies of reaction and activation are summarized in **Table S12**. **Figure 6a** shows the competitive reaction paths when the activated catalyst **3** in the presence of acetylene and H_2. Green and purple pathways represent the insertion of acetylene (**3→4**) and ethene (**3→6**), pink and black pathways represent the acetylene addition (**3→10**) and the H_2 heterolysis (**3→11**). The insertion of acetylene and ethene are both strongly exergonic reactions, and acetylene insertion are much stronger exergonic ($\Delta G_{x3\text{-}4}$ = −27.7 ~ −34.3 kcal/mol) than ethene insertion ($\Delta G_{x3\text{-}6}$ = −14.7 ~ −20.3 kcal/mol) (**Figure 6b**). Acetylene addition is endergonic for most of the activated catalysts (except for **3**, **h3**−**j3** and **m3** which are slightly exergonic), while H_2 heterolysis is endergonic for all (**3**−**m3**). The binding free energies of both acetylene and H_2 on the activated catalysts (**3**−**m3**) are smaller than that on pre-catalysts (**1**−**m**), because of the reduced electron withdrawing ability of Lewis acid site of the activated catalysts resulting from the elimination of one C_6F_5 group. The binding of acetylene on the activated catalysts are much stronger than that of H_2, which shows the similar trend as that on the pre-catalysts. However, the stronger binding of acetylene than H_2 will not cause the catalyst deactivation in particular for **3**, **d3**, **h3-m3**, because the acetylene insertion leads to the most stable products, B-vinyl intermediates (**Figure 6c**), suggesting the acetylene insertion is the dominant pathway when the activated catalysts exposed to acetylene and H_2.

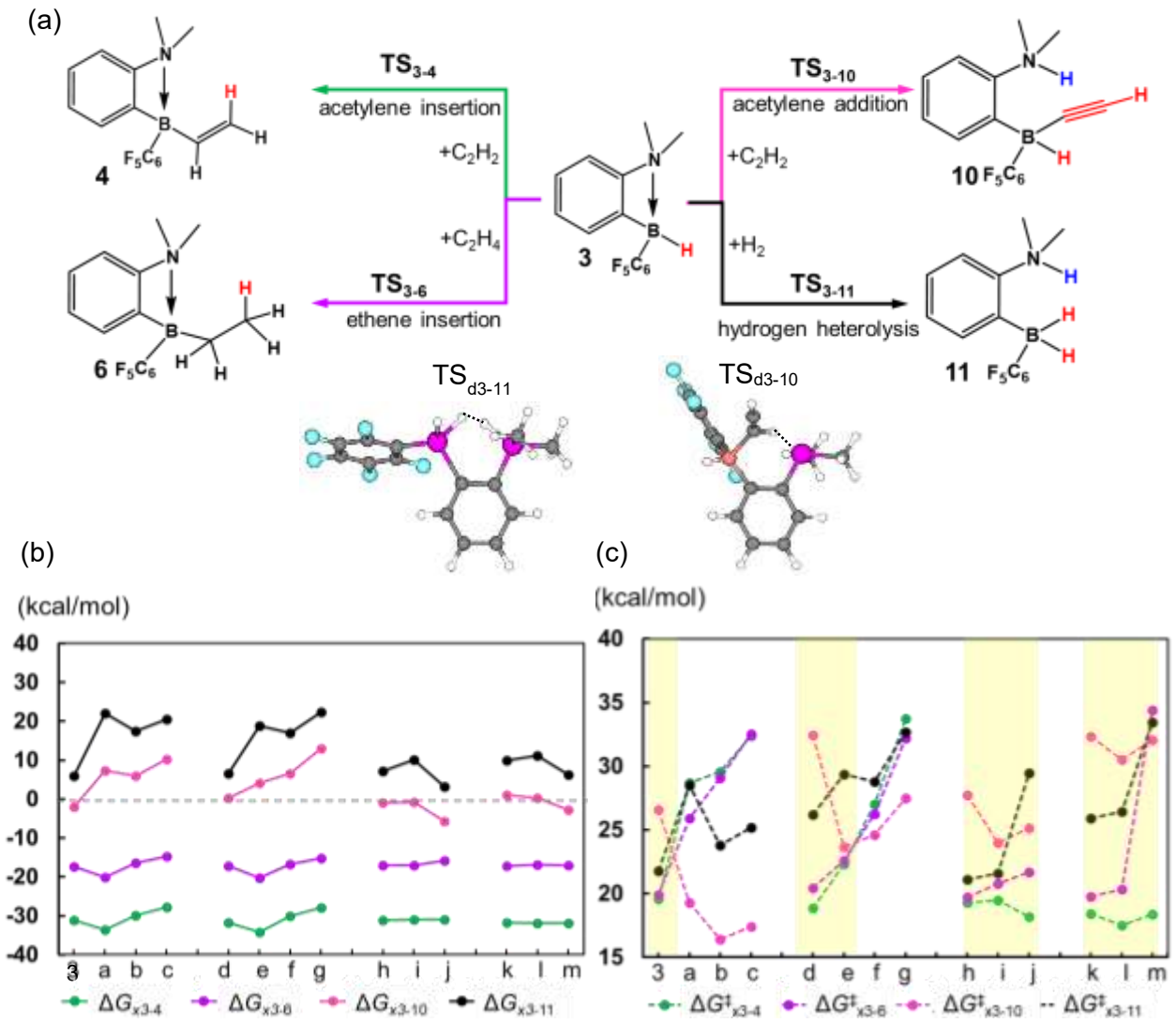

Figure 6. (a) Four possible reactions for catalyst **3**: acetylene insertion (green), ethene insertion (purple), acetylene addition (pink) and hydrogen heterolysis (black), with the structure of transition states involving in the acetylene addition and hydrogen heterolysis at **d**, (b) and (c) the Gibbs free energies of reaction and activation of the four reactions for FLP **3**-**m3**.

Our calculations demonstrate the catalyst deactivation is due to the strong binding of acetylene and the elimination of the bulky ligand at pre-activated catalyst rather than at activated catalysts. **d** and **k** could be potential catalysts that could have high selectivity and good stability for acetylene semihydrogenation.

3.4 Insights on FLP Catalysis of Terminal Alkyne Semihydrogenation

Existence of FLPs for Alkyne Semihydrogenation Since the first FLP, **1** reported by Repo and Pápai et al. in 2013 that enable the semihydrogenation of alkynes,[49] a few other FLPs

reported for this reaction.[77–80] In 2015, Du et al. reported a novel strategy of using simple alkenes as promoters for the $HB(C_6F_5)_2$-catalyzed alkynes hydrogenation.[77] In 2017, Repo and Pápai reported another new FLP for alkyne hydrogenation, 2-(Dialkylamino)phenylboranes containing the BXZ group (X, Z = C_6F_5, Cl, and H). The three FLP catalysts can only catalyze internal alkynes hydrogenation, but not terminal alkynes. Till 2020, Gellrich and coworkers reported a boroxypyridine FLP ($B(C_6F_5)_2H$/6-tert-butylpyridone), **4** (**Figure S18**), which not only show good yields and stereoselectivity for cis-selective hydrogenation of a variety of internal alkynes, but also the first time enables the metal-free semihydrogenation of terminal alkynes.[79] In analogy to boroxypyridine, Hu et al. reported a the hydrogenation of terminal alkynes catalyzed by a polymeric-BPh_3/pyridine.[80]

Reaction Mechanisms The reported FLPs capable of catalyzing semihydrogenation of alkynes are intramolecular FLPs, which could undergo two possible reaction mechanisms: intramolecular and intermolecular mechanism (**Figure 7**). Intramolecular mechanism consists of five steps: I. H_2 heterolysis, II. C_6F_5 elimination, III. alkyne insertion, IV. H_2 heterolysis and V. intramolecular protonation (left cycle), and LA and LB remain covalently connected during the reaction. While intermolecular mechanism involves LA and LB dissociation and recombination, which also consists of five steps: I. H_2 heterolysis, II′. LA-LB dissociation, III′. alkyne hydroboration, IV′. alkenylborane and pyridone combination and V′. intermolecular protonation (right cycle). The capability of the dissociation of LA-LB of FLPs plays a key role to determine the dominant reaction mechanism for the semihydrogenation of terminal alkynes. For instance, ansa-aminohydroborane FLP (coumpond **1**) reported by Repo and Pápai[49] undergoes an intramolecular mechanism because $B(C_6F_5)_2$-C_6H_4 is intact during the reaction. While boroxypyridine FLP ($B(C_6F_5)_2H$/6-tert-butylpyridone) reported by Gellrich and coworkers[79] undergoes an intermolecular mechanism because $B(C_6F_5)_2H$ is released from FLP after H_2 splitting.

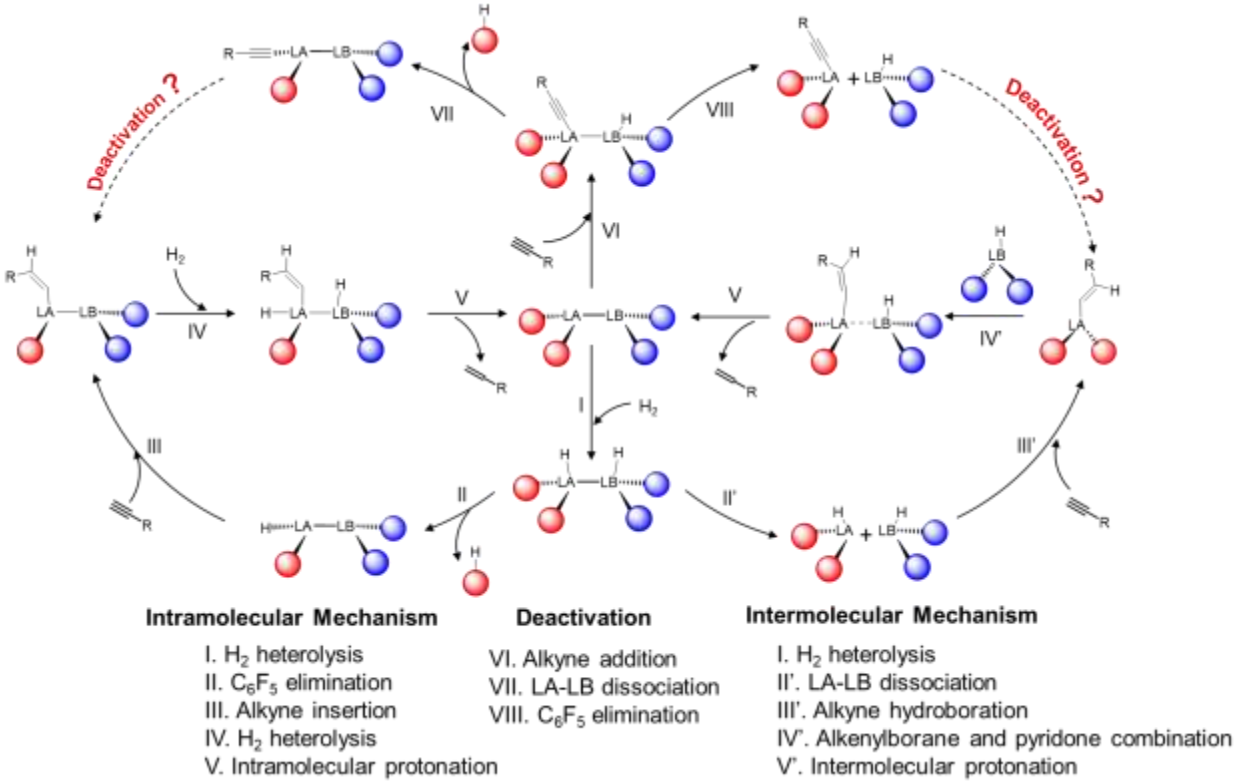

Figure 7. Two reaction mechanisms for semihydrogenation of terminal alkynes catalyzed by FLPs: intramolecular (left cycle), intermolecular (right cycle) mechanism and the pathways for the deactivation of FLPs.

FLP Deactivation Gellrich and coworkers suggested that the reversibility of the C_{sp}–H cleavage of terminal alkynes that allows H_2 activation in the presence of terminal alkynes and thus enables the hydrogenation of terminal alkynes.[79] However, we found that after the addition of terminal alkynes, the dissociation of the alkynyl borane complexes **13**–**15** ($\Delta G^{\ddagger}$=14.0(cyclohexyacetylene), 13.4(phenylacetylene), 14.7(acetylene) kcal/mol)) is more favorable than the C_{sp}–H reformation ($\Delta G^{\ddagger}$=22.9(cyclohexyacetylene), 22.7(phenylacetylene), 30.0(acetylene) kcal/mol), as shown in **Figure S18**. Our computational results suggest that the reversibility of the C_{sp}–H cleavage of terminal alkynes probably is not the key to the activity of boroxypyridine towards terminal alkynes. We explored the elimination of C_6F_5 group after the H_2 heterolysis and found that the free energy barrier is 27.7 kcal/mol (**Figure S17**), which is much higher than the H_2 splitting, alkyne addition and dissociation of pyridone borane, **4** or alkynyl borane complexes, **13**–**15**. Therefore, we believe the key for the good activity of **3** toward terminal alkyne is because of the higher activation barrier for the perfluorophenyl elimination that avoids

the catalyst degradation. In addition, the high H_2 pressure (5 bar[79]) shifts the equilibrium towards the H_2 splitting, which was also observed for FLP **1**. Therefore, H_2 heterolysis product is dominant intermediate. However, alkyne addition is inevitable which results in the maximum yield of terminal alkene product is reported to be 76% [79]. For FLP (1-NMe_2-2-$B(C_6F_5)_2$-C_6H_4, **1**), the strong terminal alkyne binding and the lower free activation barrier for the perfluorophenyl elimination results in the degradation of catalyst (**Figure S18**) and the yield of terminal alkene is zero.[49]

As shown in **Figure 7**, FLPs could be deactivated via intramolecular mechanism through two steps (VI. alkyne addition and VII. C_6F_5 elimination) or via intermolecular mechanism through three steps (VI. alkyne addition, VIII. LA-LB dissociation and VII. C_6F_5 elimination). The deactivation of FLPs for semihydrogenation of terminal alkynes due to: (1) the strong binding of terminal alkynes on FLPs with low reaction barrier, which could block the LA and LB sites for activate H_2, and (2) the low activation barrier for perfluorophenyl elimination, which results in the degradation of FLPs. One strategy to enable FLPs active towards terminal alkynes is to increase the activation energy for terminal alkyne addition and decrease the binding energy difference between H_2 and terminal alkynes, such as FLPs **d** and **k** (**Figures S19-20**). The second strategy is to increase the activation energy for C_6F_5H elimination and increase H_2 pressure. The third strategy is to weaken the binding of terminal alkynes by changing the mind their binding mode involving metal as Lewis acid site.[81]

4. Conclusions

In this work, we have designed thirteen FLPs, denoted **a**−**m**, based on the experimentally reported FLP, **1**(1-NMe_2-2-$B(C_6F_5)_2$-C_6H_4) by varying the LB site with N and P, and the LA site with B, Al, Ga and In, and replacing $-C_6F_5$ with $-C_6F_3H_2$, $-C_6H_5$, $-CF_3$. We applied density functional theory to study the activity, selectivity, and deactivation of FLPs including **1** and **a**-**m** for acetylene semihydrogenation. The catalytic cycle consists of three steps: (1) alkyne insertion, (2) H_2 heterolysis, and (3) intramolecular protonation. We calculated the free energy profile of the entire catalytic cycle and the apparent activation energies using energetic span model to estimate the activity of **1**-**m** for acetylene hydrogenation to ethene**.** We found the activity does not change much by the modification of bulky ligands, while it decreases with the direct replacement of LA and LB sites. The apparent activation energies are found to depend on step 1 (hydride insertion), and step 3 (intramolecular protonation). The activation free energies of step 1 and step 2 are both

linearly correlated with the charge of LA site. The former is a positive linear relationship because a more positively charged LA site has a stronger π donation from C≡C to FLP and weaker δ back-donation from FLP to $\pi^*_{C\equiv C}$, resulting in stronger binding of C_2H_2 at B, and thus a higher activation barrier. However, the latter is a negative linear relationship because a more positively charged LA site indicate weaker electron donation from vinyl species to LA site, resulting in a weaker LA-C bond, then a smaller free energy barrier for proton transfer to vinyl species. The selectivity was estimated by comparing the apparent activation energies for acetylene hydrogenation to ethene ($\Delta G^{\ddagger}_{C\equiv C}$) and ethene hydrogenation to ethane ($\Delta G^{\ddagger}_{C=C}$). All the FLPs designed in this work show comparable or better selectivity for semihydrogenation of acetylene comparing to **1**, except **b** and **c**. The FLPs are deactivated by the strong binding of acetylene and the elimination of electron-withdrawing bulky ligands at pre-activated catalyst rather than activated catalysts. Taking the selectivity and the stability of FLPs into account, **d** and **k** are potentially active for terminal alkynes. We review FLPs that have been experimentally reported for semihydrogenation of terminal alkynes, we summarize the most two dominant reaction mechanisms and critical factors that result in FLPs deactivation and degradation, and we provide potential strategies to avoid catalyst deactivation for terminal alkyne semihydrogenation.

■ ASSOCIATED CONTENT

Supporting Information.

The Gibbs free energy data in all the figures, Gibbs free energy profiles, descriptors, turnover frequencies, functional test data.

The xyz coordinates for all the structures are provide in the zip file named with “xyz_coordiantes.zip”

The electronic energies, enthalpies, Gibbs free energies of all the structures in both gas phase and benzene are provide in excel file named with “Energy data.xlsx”

The Supporting Information is available free of charge on the ACS Publications website at DOI: 10.1021/

■ AUTHOR INFORMATION

Corresponding Authors

*E-mail: Jingyun Ye: yej1@duq.edu

ORCID

Jingyun Ye: 0000-0003-4373-9625

Notes

The authors declare no competing financial interest.

■ ACKNOWLEDGMENTS

This research was supported by the start-up fund of Duquesne University and Clarkson University, and in part by the by the U.S. Department of Energy, Office of Basic Energy Sciences, Division of Chemical Sciences, Geosciences, and Biosciences under award DE-FG02-17ER16362 to the Nanoporous Materials Genome Center as part of the Computational Chemical Sciences Program. The DFT computations were performed at the Extreme Science and Engineering Discovery Environment (XSEDE) under project TG-CHE200106. Megan McEwen is supported in part by the Walsh undergraduate research fellowship of Clarkson University and the award DE-FG02-17ER16362.

Reference

(1) Bonrath, W.; Medlock, J.; Schütz, J.; Wüstenberg, B.; Netscher, T. Hydrogenation in the Vitamins and Fine Chemicals Industry – An Overview. *Hydrogenation* **2012**, 69-90.

(2) Chen, B.; Dingerdissen, U.; Krauter, J. G. E.; Lansink Rotgerink, H. G. J.; Möbus, K.; Ostgard, D. J.; Panster, P.; Riermeier, T. H.; Seebald, S.; Tacke, T.; et al. New Developments in Hydrogenation Catalysis Particularly in Synthesis of Fine and Intermediate Chemicals. *Appl. Catal. A Gen.* **2005**, *280*, 17–46.

(3) Bonrath, W.; Netscher, T. Catalytic Processes in Vitamins Synthesis and Production. *Appl. Catal. A Gen.* **2005**, *280*, 55–73.

(4) Saudan, L. A. Hydrogenation Processes in the Synthesis of Perfumery Ingredients. *Acc. Chem. Res.* **2007**, *40*, 1309–1319.

(5) Borodziński, A.; Bond, G. C. Selective Hydrogenation of Ethyne in Ethene-Rich Streams on Palladium Catalysts. Part 1. Effect of Changes to the Catalyst During Reaction. *Catal. Rev.* **2007**, *48*, 91–144.

(6) Eggersdorfer, M.; Laudert, D.; Létinois, U.; McClymont, T.; Medlock, J.; Netscher, T.; Bonrath, W. One Hundred Years of Vitamins - A Success Story of the Natural Sciences. *Angew. Chem. Int. Ed*. **2012**, 12960–12990.

(7) Borodziński, A.; Bond, G. C. Selective Hydrogenation of Ethyne in Ethene-Rich Streams

on Palladium Catalysts, Part 2: Steady-State Kinetics and Effects of Palladium Particle Size, Carbon Monoxide, and Promoters. *Catal. Rev.* **2008**, *50*, 379–469.

(8) Molnár, Á.; Sárkány, A.; Varga, M. Hydrogenation of Carbon–Carbon Multiple Bonds: Chemo-, Regio- and Stereo-Selectivity. *J. Mol. Catal. A Chem.* **2001**, *173*, 185–221.

(9) Gerhard Ertl, Helmut Knözinger, Ferdi Schüth, J. W. Handbook of Heterogeneous Catalysis, 2nd Edition, Wiley. **2009**, *48*, 3390−3391.

(10) Galvis, H. M. T.; Jong, K. P. de. Catalysts for Production of Lower Olefins from Synthesis Gas: A Review. *ACS Catal.* **2013**, *3*, 2130–2149.

(11) Armbrüster, M.; Kovnir, K.; Friedrich, M.; Teschner, D.; Wowsnick, G.; Hahne, M.; Gille, P.; Szentmiklósi, L.; Feuerbacher, M.; Heggen, M.; et al. $Al_{13}Fe_4$ as a Low-Cost Alternative for Palladium in Heterogeneous Hydrogenation. *Nat. Mater.* **2012**, *11*, 690–693.

(12) Zacharopoulou, V.; Lemonidou, A. A. Olefins from Biomass Intermediates: A Review. *Catalysts* **2018**, *8*, 2.

(13) Fakhroleslam, M.; Sadrameli, S. M. Thermal Cracking of Hydrocarbons for the Production of Light Olefins; A Review on Optimal Process Design, Operation, and Control. *Ind. Eng. Chem. Res.* **2020**, *59*, 12288–12303.

(14) Noemí S. Schbib; Miguel A. García; Carlos E. Gígola, and; Errazu, A. F. Kinetics of Front-End Acetylene Hydrogenation in Ethylene Production. *Ind. Eng. Chem. Res.* **1996**, *35*, 1496–1505.

(15) Nikolaev, S. A.; Zanaveskin, L. N.; Smirnov, V. V; Averyanov, V. A.; Zanaveskin, K. L. Catalytic Hydrogenation of Alkyne and Alkadiene Impurities from Alkenes. Practical and Theoretical Aspects. *Russ. Chem. Rev.* **2009**, *78*, 231–247.

(16) Huang, L.; Subramanian, R.; Wang, J.; Kwon Oh, J.; Ye, Z. Ligand Screening for Palladium Nanocatalysts towards Selective Hydrogenation of Alkynes. *Mol. Catal.* **2020**, *488*, 110923.

(17) Chung, J.; Kim, C.; Jeong, H.; Yu, T.; Binh, D. H.; Jang, J.; Lee, J.; Kim, B. M.; Lim, B. Selective Semihydrogenation of Alkynes on Shape-Controlled Palladium Nanocrystals. *Chem. – An Asian J.* **2013**, *8*, 919–925.

(18) Chen, C.; Ou, W.; Yam, K.-M.; Xi, S.; Zhao, X.; Chen, S.; Li, J.; Lyu, P.; Ma, L.; Du, Y.; et al. Zero-Valent Palladium Single-Atoms Catalysts Confined in Black Phosphorus for

Efficient Semi-Hydrogenation. *Adv. Mater.* **2021**, *33*, 2008471.

(19) Akl, D. F.; Ruiz-Ferrando, A.; Fako, E.; Hauert, R.; Safonova, O.; Mitchell, S.; López, N.; Pérez-Ramírez, J. Precursor Nuclearity and Ligand Effects in Atomically-Dispersed Heterogeneous Iron Catalysts for Alkyne Semi-Hydrogenation. *ChemCatChem* **2021**, *13*, 3247–3256.

(20) Li, Z.; Ren, Q.; Wang, X.; Chen, W.; Leng, L.; Zhang, M.; Horton, J. H.; Liu, B.; Xu, Q.; Wu, W.; et al. Highly Active and Stable Palladium Single-Atom Catalyst Achieved by a Thermal Atomization Strategy on an SBA-15 Molecular Sieve for Semi-Hydrogenation Reactions. *ACS Appl. Mater. Interfaces* **2021**, *13*, 2530–2537.

(21) Guo, Y.; Qi, H.; Su, Y.; Jiang, Q.; Cui, Y.-T.; Li, L.; Qiao, B. Front Cover: High Performance of Single-Atom Catalyst Pd_1/MgO for Semi-Hydrogenation of Acetylene to Ethylene in Excess Ethylene. *ChemNanoMat* **2021**, *7*, 488–488.

(22) Kuo, C.-T.; Lu, Y.; Kovarik, L.; Engelhard, M.; Karim, A. M. Structure Sensitivity of Acetylene Semi-Hydrogenation on Pt Single Atoms and Subnanometer Clusters. *ACS Catal.* **2019**, 11030–11041.

(23) Bakuru, V. R.; Samanta, D.; Maji, T. K.; Kalidindi, S. B. Transfer Hydrogenation of Alkynes into Alkenes by Ammonia Borane over Pd-MOF Catalysts. *Dalt. Trans.* **2020**, *49*, 5024–5028.

(24) Li, J. H.; Yu, Z. W.; Gao, Z.; Li, J. Q.; Tao, Y.; Xiao, Y. X.; Yin, W. H.; Fan, Y. L.; Jiang, C.; Sun, L. J.; et al. Ultralow-Content Palladium Dispersed in Covalent Organic Framework for Highly Efficient and Selective Semihydrogenation of Alkynes. *Inorg. Chem.* **2019**, *58*, 10829–10836.

(25) Weerachawanasak, P.; Mekasuwandumrong, O.; Arai, M.; Fujita, S. I.; Praserthdam, P.; Panpranot, J. Effect of Strong Metal–Support Interaction on the Catalytic Performance of Pd/TiO_2 in the Liquid-Phase Semihydrogenation of Phenylacetylene. *J. Catal.* **2009**, *262*, 199–205.

(26) He, Y.; Fan, J.; Feng, J.; Luo, C.; Yang, P.; Li, D. Pd Nanoparticles on Hydrotalcite as an Efficient Catalyst for Partial Hydrogenation of Acetylene: Effect of Support Acidic and Basic Properties. *J. Catal.* **2015**, *331*, 118–127.

(27) Cao, Y.; Fu, W.; Ren, Z.; Sui, Z.; Zhou, J.; Luo, J.; Duan, X.; Zhou, X. Tailoring Electronic Properties and Kinetics Behaviors of Pd/N-CNTs Catalysts for Selective

Hydrogenation of Acetylene. *AIChE J.* **2020**, *66*, e16857.

(28) Shao, L.; Zhang, B.; Zhang, W.; Teschner, D.; Girgsdies, F.; Schlögl, R.; Su, D. S. Improved Selectivity by Stabilizing and Exposing Active Phases on Supported Pd Nanoparticles in Acetylene-Selective Hydrogenation. *Chem. – A Eur. J.* **2012**, *18*, 14962–14966.

(29) Benavidez, A. D.; Burton, P. D.; Nogales, J. L.; Jenkins, A. R.; Ivanov, S. A.; Miller, J. T.; Karim, A. M.; Datye, A. K. Improved Selectivity of Carbon-Supported Palladium Catalysts for the Hydrogenation of Acetylene in Excess Ethylene. *Appl. Catal. A Gen.* **2014**, *482*, 108–115.

(30) Verho, O.; Zheng, H.; Gustafson, K. P. J.; Nagendiran, A.; Zou, X.; Bäckvall, J.-E. Application of Pd Nanoparticles Supported on Mesoporous Hollow Silica Nanospheres for the Efficient and Selective Semihydrogenation of Alkynes. *ChemCatChem* **2016**, *8*, 773–778.

(31) Cordoba, M.; Coloma-Pascual, F.; Quiroga, M. E.; Lederhos, C. R. Olefin Purification and Selective Hydrogenation of Alkynes with Low Loaded Pd Nanoparticle Catalysts. *Ind. Eng. Chem. Res.* **2019**, *58*, 17182–17194.

(32) Deng, D.; Yang, Y.; Gong, Y.; Li, Y.; Xu, X.; Wang, Y. Palladium Nanoparticles Supported on Mpg-C3N4 as Active Catalyst for Semihydrogenation of Phenylacetylene under Mild Conditions. *Green Chem.* **2013**, *15*, 2525–2531.

(33) Hu, M.; Zhang, J.; Zhu, W.; Chen, Z.; Gao, X.; Du, X.; Wan, J.; Zhou, K.; Chen, C.; Li, Y. 50 Ppm of Pd Dispersed on $Ni(OH)_2$ Nanosheets Catalyzing Semi-Hydrogenation of Acetylene with High Activity and Selectivity. *Nano Res.* **2017**, *11*, 905–912.

(34) Niu, W.; Gao, Y.; Zhang, W.; Yan, N.; Lu, X. Pd–Pb Alloy Nanocrystals with Tailored Composition for Semihydrogenation: Taking Advantage of Catalyst Poisoning. *Angew. Chem. Int. Ed.* **2015**, *54*, 8271–8274.

(35) Zheng, Y.; Tan, T.; Wang, C. Seed-Mediated Growth of Alloyed Ag-Pd Shells toward Alkyne Semi-Hydrogenation Reactions under Mild Conditions. *Chinese J. Chem.* **2021**, *39*, 3071–3078.

(36) Li, Z.; Hu, M.; Liu, B.; Liu, J.; Wang, P.; Yao, J.; Zhang, X.; He, M.; Song, W. Pd−Zn Alloy Nanoparticles Encapsulated into Mesoporous Silica with Confinement Effect for Highly Selective Semi-Hydrogenation of Phenylacetylene. *ChemCatChem* **2021**, *13*, 868–

873.

(37) Lini Yang; Yushu Guo; Jun Long; Lixin Xia; Dan Li; Jianping Xiao; Hongyang Liu. PdZn Alloy Nanoparticles Encapsulated within a Few Layers of Graphene for Efficient Semi-Hydrogenation of Acetylene. *Chem. Commun.* **2019**, *55*, 14693–14696.

(38) Sárkány, A.; Geszti, O.; Sáfrán, G. Preparation of Pdshell–Aucore/SiO_2 Catalyst and Catalytic Activity for Acetylene Hydrogenation. *Appl. Catal. A Gen.* **2008**, *350*, 157–163.

(39) Ma, L.; Jiang, P.; Wang, K.; Lan, K.; Huang, X.; Yang, M.; Gong, L.; Jia, Q.; Mu, X.; Xiong, Y.; et al. Phosphorus and Nitrogen-Doped Palladium Nanomaterials Support on Coral-like Carbon Materials as the Catalyst for Semi-Hydrogenation of Phenylacetylene and Mechanism Study. *J. Alloys Compd.* **2021**, *868*, 159047.

(40) Huang, L.; Hu, K.; Ye, G.; Ye, Z. Highly Selective Semi-Hydrogenation of Alkynes with a Pd Nanocatalyst Modified with Sulfide-Based Solid-Phase Ligands. *Mol. Catal.* **2021**, *506*, 111535.

(41) Cao, Y.; Zhang, H.; Ji, S.; Sui, Z.; Jiang, Z.; Wang, D.; Zaera, F.; Zhou, X.; Duan, X.; Li, Y. Adsorption Site Regulation to Guide Atomic Design of Ni–Ga Catalysts for Acetylene Semi-Hydrogenation. *Angew. Chem. Int. Ed.* **2020**, *59*, 11647–11652.

(42) Desai, S. P.; Ye, J.; Zheng, J.; Ferrandon, M. S.; Webber, T. E.; Platero-Prats, A. E.; Duan, J.; Garcia-Holley, P.; Camaioni, D. M.; Chapman, K. W.; et al. Well-Defined Rhodium–Gallium Catalytic Sites in a Metal–Organic Framework: Promoter-Controlled Selectivity in Alkyne Semihydrogenation to E-Alkenes. *J. Am. Chem. Soc.* **2018**, *140*, 15309–15318.

(43) Wang, Z.; Garg, A.; Wang, L.; He, H.; Dasgupta, A.; Zanchet, D.; Janik, M. J.; Rioux, R. M.; Román-Leshkov, Y. Enhancement of Alkyne Semi-Hydrogenation Selectivity by Electronic Modification of Platinum. *ACS Catal.* **2020**, *10*, 6763–6770.

(44) Song, L.; Feng, Q.; Wang, Y.; Ding, S.; Wu, Y.-D.; Zhang, X.; Chung, L. W.; Sun, J. Ru-Catalyzed Migratory Geminal Semihydrogenation of Internal Alkynes to Terminal Olefins. *J. Am. Chem. Soc.* **2019**, *141*, 17441–17451.

(45) Stephan, D. W. The Broadening Reach of Frustrated Lewis Pair Chemistry. *Science*, **2016**, *354*, aaf7229.

(46) Stephan, D. W. Frustrated Lewis Pairs. *J. Am. Chem. Soc.*, **2015**, *137*, 10018–10032.

(47) Stephan, D. W. Frustrated Lewis Pairs: From Concept to Catalysis. *Acc. Chem. Res.* **2015**,

48, 306–316.

(48) Stephan, D. W. Frustrated Lewis Pair Catalysis: An Introduction; Springer, Cham, 2021, 1–28.

(49) K, C.; A, M.; I, P.; M, N.; M, L.; T, R. A Frustrated-Lewis-Pair Approach to Catalytic Reduction of Alkynes to Cis-Alkenes. *Nat. Chem.* **2013**, *5*, 718–723.

(50) Frisch, M. J.; Trucks, G. W.; Schlegel, H. B.; Scuseria, G. E.; Robb, M. A.; Cheeseman, J. R.; Scalmani, G.; Barone, V.; Mennucci, B.; Petersson, G. A.; et al. Gaussian 09 Revision B.01, 2009.

(51) Zhao, Y.; Truhlar, D. G. The M06 Suite of Density Functionals for Main Group Thermochemistry, Thermochemical Kinetics, Noncovalent Interactions, Excited States, and Transition Elements: Two New Functionals and Systematic Testing of Four M06-Class Functionals and 12 Other Function. *Theor. Chem. Acc.* **2008**, *120*, 215–241.

(52) Weigend, F. Accurate Coulomb-Fitting Basis Sets for H to Rn. *Phys. Chem. Chem. Phys.* **2006**, *8*, 1057–1065.

(53) Weigend, F.; Ahlrichs, R. Balanced Basis Sets of Split Valence, Triple Zeta Valence and Quadruple Zeta Valence Quality for H to Rn: Design and Assessment of Accuracy. *Phys. Chem. Chem. Phys.* **2005**, *7*, 3297–3305.

(54) Marenich, A. V.; Cramer, C. J.; Truhlar, D. G. Universal Solvation Model Based on Solute Electron Density and on a Continuum Model of the Solvent Defined by the Bulk Dielectric Constant and Atomic Surface Tensions. *J. Phys. Chem. B* **2009**, *113*, 6378–6396.

(55) Marenich, A. V.; Jerome, S. V.; Cramer, C. J.; Truhlar, D. G. Charge Model 5: An Extension of Hirshfeld Population Analysis for the Accurate Description of Molecular Interactions in Gaseous and Condensed Phases. *J. Chem. Theory Comput.* **2012**, *8*, 527–541.

(56) Zhao, Y.; Truhlar, D. G. A New Local Density Functional for Main-Group Thermochemistry, Transition Metal Bonding, Thermochemical Kinetics, and Noncovalent Interactions. *J. Chem. Phys.* **2006**, *125*, 194101.

(57) Alecu, I. M.; Zheng, J.; Zhao, Y.; Truhlar, D. G. Computational Thermochemistry: Scale Factor Databases and Scale Factors for Vibrational Frequencies Obtained from Electronic Model Chemistries. *J. Chem. Theory Comput.* **2010**, *6*, 2872–2887.

(58) Mitoraj, M.; Michalak, A. Natural Orbitals for Chemical Valence as Descriptors of Chemical Bonding in Transition Metal Complexes. *J. Mol. Model.* **2007**, *13*, 347–355.

(59) Michalak, A.; Mariusz Mitoraj, A.; Ziegler, T. Bond Orbitals from Chemical Valence Theory. *J. Phys. Chem. A,* **2008**, *112*, 1933–1939.

(60) Mitoraj, M.; Michalak, A. Donor–Acceptor Properties of Ligands from the Natural Orbitals for Chemical Valence. *Organometallics* **2007**, *26*, 6576–6580.

(61) Ziegler, T.; Rauk, A. A Theoretical Study of the Ethylene-Metal Bond in Complexes between Copper(1+), Silver(1+), Gold(1+), Platinum(0) or Platinum(2+) and Ethylene, Based on the Hartree-Fock-Slater Transition-State Method. *Inorg. Chem.* **1979**, *18*, 1558–1565.

(62) Ziegler, T.; Rauk, A. Carbon Monoxide, Carbon Monosulfide, Molecular Nitrogen, Phosphorus Trifluoride, and Methyl Isocyanide as .Sigma. Donors and .Pi. Acceptors. A Theoretical Study by the Hartree-Fock-Slater Transition-State Method. *Inorg. Chem.* **1979**, *18*, 1755–1759.

(63) Mitoraj, M. P. Bonding in Ammonia Borane: An Analysis Based on the Natural Orbitals for Chemical Valence and the Extended Transition State Method (ETS-NOCV). *J. Phys. Chem. A* **2011**, *115*, 14708–14716.

(64) Te Velde, G.; Bickelhaupt, F. M.; Baerends, E. J.; Fonseca Guerra, C.; van Gisbergen, S. J. A.; Snijders, J. G.; Ziegler, T. Chemistry with ADF. *J. Comput. Chem.* **2001**, *22*, 931–967.

(65) Fonseca Guerra, C.; Snijders, J. G.; te Velde, G.; Baerends, E. J. Towards an Order- N DFT Method. *Theor. Chem. Accounts Theory, Comput. Model.* **1998**, *99*, 391–403.

(66) Baerends, E. J.; Ziegler, T.; Atkins, A. J.; Autschbach, J.; Bashford, D.; Baseggio, O.; Bérces, A.; Bickelhaupt, F. M.; Bo, C.; Boerritger, P. M.; et al. ADF2017, SCM, Theoretical Chemistry, Vrije Universiteit, Amsterdam, The Netherlands, Https://Www.Scm.Com.

(67) Chong, D. P. Augmenting Basis Set for Time-Dependent Density Functional Theory Calculation of Excitation Energies: Slater-Type Orbitals for Hydrogen to Krypton. *Mol. Phys.* **2005**, *103*, 749–761.

(68) Ye, J.; Li, L.; Johnson, J. K. The Effect of Topology in Lewis Pair Functionalized Metal Organic Frameworks on CO_2 Adsorption and Hydrogenation. *Catal. Sci. Technol.* **2018**, *8*,

4609–4617.

(69) Kozuch, S.; Shaik, S. A Combined Kinetic−Quantum Mechanical Model for Assessment of Catalytic Cycles: Application to Cross-Coupling and Heck Reactions. *J. Am. Chem. Soc.* **2006**, *128*, 3355–3365.

(70) Kozuch, S.; Shaik, S. How to Conceptualize Catalytic Cycles? The Energetic Span Model. *Acc. Chem. Res.* **2011**, *44*, 101–110.

(71) Hansmann, M. M.; Melen, R. L.; Rudolph, M.; Rominger, F.; Wadepohl, H.; Stephan, D. W.; Hashmi, A. S. K. Cyclopropanation/Carboboration Reactions of Enynes with $B(C_6F_5)_3$. *J. Am. Chem. Soc.* **2015**, *137*, 15469–15477.

(72) Ma, Y.; Lou, S. J.; Luo, G.; Luo, Y.; Zhan, G.; Nishiura, M.; Luo, Y.; Hou, Z. B(C6F5)3/Amine-Catalyzed C(Sp)−H Silylation of Terminal Alkynes with Hydrosilanes: Experimental and Theoretical Studies. *Angew. Chem. Int. Ed.* **2018**, *57*, 15222–15226.

(73) Bismuto, A.; Nichol, G. S.; Duarte, F.; Cowley, M. J.; Thomas, S. P. Characterization of the Zwitterionic Intermediate in 1,1-Carboboration of Alkynes. *Angew. Chem. Int. Ed.* **2020**, *59*, 12731–12735.

(74) Brar, A.; Mummadi, S.; Unruh, D. K.; Krempner, C. Verkade Base in FLP Chemistry-From Stoichiometric C-H Bond Cleavage to the Catalytic Dimerization of Alkynes. *Organometallics* **2020**, *39*, 4307–4311.

(75) Mömming, C. M.; Kehr, G.; Wibbeling, B.; Fröhlich, R.; Schirmer, B.; Grimme, S.; Erker, G. Formation of Cyclic Allenes and Cumulenes by Cooperative Addition of Frustrated Lewis Pairs to Conjugated Enynes and Diynes. *Angew. Chem. Int. Ed.* **2010**, *49*, 2414–2417.

(76) Dureen, M. A.; Stephan, D. W. Terminal Alkyne Activation by Frustrated and Classical Lewis Acid/Phosphine Pairs. *J. Am. Chem. Soc.* **2009**, *131*, 8396–8397.

(77) Liu, Y.; Hu, L.; Chen, H.; Du, H. An Alkene-Promoted Borane-Catalyzed Highly Stereoselective Hydrogenation of Alkynes to Give Z- and E-Alkenes. *Chem. – A Eur. J.* **2015**, *21*, 3495–3501.

(78) Chernichenko, K.; Kótai, B.; Nieger, M.; Heikkinen, S.; Pápai, I.; Repo, T. Replacing C6F5 Groups with Cl and H Atoms in Frustrated Lewis Pairs: H_2 Additions and Catalytic Hydrogenations. *Dalt. Trans.* **2017**, *46*, 2263–2269.

(79) Wech, F.; Hasenbeck, M.; Gellrich, U. Semihydrogenation of Alkynes Catalyzed by a

Pyridone Borane Complex: Frustrated Lewis Pair Reactivity and Boron–Ligand Cooperation in Concert. *Chem. – A Eur. J.* **2020**, *26*, 13445–13450.

(80) Liu, Q.; Yang, L.; Yao, C.; Geng, J.; Wu, Y.; Hu, X. Controlling the Lewis Acidity and Polymerizing Effectively Prevent Frustrated Lewis Pairs from Deactivation in the Hydrogenation of Terminal Alkynes. *Org. Lett.* **2021**, *23*, 3685–3690.

(81) Hidalgo, N.; Moreno, J. J.; Pérez-Jiménez, M.; Maya, C.; López-Serrano, J.; Campos, J. Tuning Activity and Selectivity during Alkyne Activation by Gold(I)/Platinum(0) Frustrated Lewis Pairs. *Organometallics* **2020**, *39*, 2534–2544.

TOC Graphic: